Title

A Hybrid Redox-Supercapacitor System with Anionic Catholyte and Cationic Anolyte

Journal

Journal of The Electrochemical Society, 161(6)

ISSN

0013-4651

Authors

Wang, B
Maciá-Agulló, JA
Prendiville, DG
et al.

Publication Date

2014

DOI

10.1149/2.058406jes

A Hybrid Redox-Supercapacitor System with Anionic Catholyte and Cationic Anolyte

B. Wang,[b] J. A. Maciá-Agulló,[a,d] D. G. Prendiville,[a] X. Zheng,[a] D. Liu,[a] Y. Zhang,[a]

S. W. Boettcher,[c] X. Ji,[b] G. D. Stucky[a]

[a] Department of Chemistry and Biochemistry, University of California, Santa Barbara, California, 93106-9510, USA

[b] Department of Chemistry, Oregon State University, Corvallis, Oregon 97331-4003, USA

[c] Department of Chemistry and Biochemistry, University of Oregon, Eugene, Oregon, 97403, USA

[d] Instituto Nacional del Carbón (CSIC). P. O. Box 73, 33080 Oviedo, Spain

Abstract

A significant challenge for energy storage technologies is to realize battery-level energy density and capacitor-level durability and power density in one device. By introducing an electrolyte composed of an anionic catholyte and a cationic anolyte into a symmetric carbon-based supercapacitor configuration, a hybrid electrochemical battery-supercapacitor system using soluble redox species delivers significantly improved energy density from 20 to 42 W•h/kg (based on the electrode mass) and stable capacities for > 10^4 cycles. The ionic species formed in the electrolyte are studied by UV-Vis, Raman and mass spectroscopy to probe the energy storage mechanism. The strategy is general and may provide a route to critically-needed fast-charging devices with both high energy density and power.

Electrochemical devices deliver energy via spontaneous electron migration from one electrode to the other through an external circuit, driven either by Faradaic reactions, e.g. in batteries, or by polarization,[1] e.g. in electrical double layer capacitors (EDLCs).[2-5] In a battery, solid-state Faradaic processes often lead to poor cycling reversibility and limited power performance.[6] Operation of EDLCs involves neither inter-electrode mass transfer nor solid-state ion diffusion, which leads to long cycling life and high-power.[7,8] Significant progress has been made to EDLCs in terms of power densities and physical flexibility.[9-19] Unfortunately, the low energy densities of EDLCs, typically < 5 W•h/kg, seriously limit applications.[5] In order to increase the energy density, redox-active oxides, e.g. RuO_2 or MnO_2, have been added to electrodes to provide so-called "pseudo-capacitance" associated with the resulting surface Faradaic redox chemistry.[20-28] These devices exhibit compromised power performance and cycle lifetime, compared to EDLCs. Recently, incorporating solvated redox-active species into electrolytes has been reported to improve charge storage.[24, 29, 30] One advantage of using soluble redox species is that the charge/discharge processes do not involve solid-state reactions or solid-state diffusion. Frackowiak et al. reported a capacitor using KI and $VOSO_4$ solutions separated by a Nafion membrane into two compartments of a cell, as catholyte and anolyte, respectively.[31] Enhanced energy density was observed.

We report a hybrid electrochemical battery-supercapacitor system using soluble redox species. The proposed system integrates both Faradaic and capacitive energy storage in the same device. We hypothesize that the polarized electrodes in the charged cell retard diffusion of the oppositely charged redox ions to mitigate self-discharge, and show that the cell does not need the ion-selective membrane as a separator for short-time-scale energy storage. During charging, the KI/$VOSO_4$ electrolyte evolves into both catholyte and anolyte, as schematically shown in

Figure 1. The device, as simple as an EDLC, involves no solid-state phenomena during operation, no ion-selective membrane separator, and a single electrolyte. Stable cycling life (10,000 cycles) and high energy density (20 to 42 W•h/kg) are demonstrated.

Experimental

Carbon activation. Physical activation by CO_2 oxidation was employed to generate porosity in the carbon fibres. Carbon fibres (Donacarbo S-241 from Osaka gas Co., Ltd), 2 g, were placed into a tube furnace. The furnace was purged with nitrogen gas at a flow rate of 100 mL/min for 30 min. Then, the temperature was increased at 5 °C/min to the desired activation temperature, i.e. 890 °C. Once the activation temperature was reached, the nitrogen flow was switched to CO_2, and the annealing was continued for another 22.5 hrs under CO_2 at a flow rate of 100 mL/min.

Characterization of carbon porosity. The porosity of the activated carbons was characterized by N_2 adsorption at –196 °C by a Micromeritics TriStar II 3020 analyzer. Samples were outgassed at 250 °C for 4 hrs before the measurements. Nitrogen adsorption results were used to determine specific BET surface area and pore volumes. Pore size distributions are obtained applying the DFT method to the isotherms using the software supplied by Micromeritics.

Mass spectrometry analysis. Mass spectra were recorded by a traveling-wave Q-TOF mass spectrometer (Water Synapt Prototype) [Pringle, S. D. et al. Int. J. Mass Spectrom. 261, 1-12 (2007)]. For the mass spectrometry analysis, ions are generated continuously by a nanoelectrospray ionization source and transmitted into and through the first part of the mass spectrometer including T-wave ion guides, quadrupole ion guide which works in radio-frequency

(RF)-only mode and ion mobility spectrometry (IMS) cell. The ions undergo collisions with neutral gas molecules (i.e. N_2 gas) to reduce both energy spread and the beam diameter for better transmission. The ions were analyzed by orthogonal acceleration (oa) time-of-flight (TOF) analyzer where the ions were separated and recorded based on their mass-to-charge ratios (m/z).

Electrochemical Measurements . The carbon and PVDF binder (polyvinylidene fluoride) in a weight ratio of 9/1 was sonicated in cyclopentanone for 2 hours to obtain a fine dispersion. The suspension obtained was drop-casted onto carbon-fiber papers as electrodes. The load is 1 mg/cm^2 for carbon active mass. Swagelok® cells of a two-electrode configuration were assembled for electrochemical measurements. The active mass loading in the electrodes of the H-cell is also 1 mg/cm^2. H-cell contains much more electrolyte than Swagelok® cells so that the electrolyte can be analyzed. Whatman® filter paper was used as the separator. All electrochemical measurements were carried out on an EC-lab VMP3 instrument at room temperature. The specific charge storage on the x-axis is calculated by $I \times \Delta t$, where I is 1 A/g, and Δt is the discharge duration. The integral of $Vq \bullet dq$, which is the area below a discharge curve, represents the electric energy output by a cell. The energy densities were calculated by integration of the discharge curves based on the mass only from both electrodes for cells with different electrolytes measured at the current rate of 1 A/g.

Results and Discussion

We studied symmetric carbon-based two-electrode Swagelok® cells containing both KI and $VOSO_4$ of different concentrations with a molar ratio of 3:2. We used activated carbon fibers[32] as the electrode material with a specific Brunauer-Emmet-Teller (BET) surface area of 2576 m^2/g. Figure S1 shows a type-I isotherm, the pore size distribution, and the morphology of

the carbon. The cells only differ in the electrolyte used, and we refer to them by their electrolyte salts and concentrations.

Cyclic voltammetry (CV) and galvanostatic measurements were conducted to compare the performance of different electrolytes. As can be seen in Figure 2a, the H_2SO_4 (1 M) cell exhibits a typical capacitive CV while the [KI (0.15 M) + $VOSO_4$ (0.1 M)] cell exhibits peaks in the CV at the same rate of 20 mV/s and a much larger area enclosed in the CV curve, indicating Faradaic redox behavior. A CV curve at a slow rate of 0.5 mV/s reveals that there are two sets of redox reactions, one centered 0.05 V and the other centered at 0.33 V (see Figure S2). As seen in Figure 2b, the voltage of the H_2SO_4 (1 M) cell is a quasi-linear function of the charge stored, characteristic of simple capacitive behavior. The energy density is calculated to be 3.6 W•h/kg, a typical value for EDLC using aqueous electrolyte. The energy densities were improved to 5.2 W•h/kg for the KI (0.15 M) cell and 7.5 W•h/kg for the $VOSO_4$ (0.1 M) cell.

Cells containing either KI or $VOSO_4$ exhibit approximately a linear voltage as a function of the stored charge, similar to hydroquinone-mediated EDLCs.[33] Interestingly, when only one redox-active ion is introduced (either I^- or VO^{2+}), the cell discharge profile roughly reflects the capacitive process of the other electrode. The discharge curves (Figure 2c) of [KI + $VOSO_4$] cells show distinct redox plateaus. The plateau is observed due to the slower rate of change in potential for the redox reactions according to the Nernst Equation than for the rate of change in potential that arises from the charge/discharge processes of electrical double layers. For the [KI (0.75 M) + $VOSO_4$ (0.5 M)] cell, the energy density reaches 42 W•h/kg. The charge storage and energy density of [KI + $VOSO_4$] cells increase when the concentrations of the active species are higher, but are not proportional to the concentration. Note that the [KI (3 M) + $VOSO_4$ (2 M)] cell cannot be polarized to a cell voltage of 1.0 V (Figure S3) at a current of 1 A/g. This may be

due to the more pronounced self-discharge of the redox species when the concentration is high. Due to the poor cycling stability of the [KI (0.75 M), $VOSO_4$ (0.5 M)] cell, we chose to further investigate the rate performance of the [KI (0.3 M) + $VOSO_4$ (0.2 M)] cell. The charge storage capacity was well maintained when rates are doubled and quadrupled (Figure 2d).

The aforementioned results demonstrate that solvated redox-active ions contribute to the high energy density of the hybrid battery-supercapacitor system. Note that the sum of the capacities of the [KI (0.15 M)] cell and the [$VOSO_4$ (0.1 M)] cell, 236 C/g, is much less than the capacity of the [KI (0.15 M), $VOSO_4$ (0.1 M)] cell, 384 C/g (Table S1).[34, 35] This high capacity can be attributed to new ions formed by reactions between KI and $VOSO_4$, which are discussed below. Full charge/discharge curves of electrolytes with different salt concentrations are shown in Figure S4. We further tested the galvanostatic cycling (Figure 2e) of the [KI (0.3 M) + $VOSO_4$ (0.2 M)] cell at a current density of 4 A/g. Surprisingly, the charge storage capacity slowly increased upon cycling in the first 2000 cycles to 400 C/g. The increase may be caused by the formation of new redox-active ions in the electrolyte. The energy density of this new system is comparable to pseudocapacitor systems that use symmetric oxides/oxides or hybrid oxides/carbon-based materials.[36] The >10,000-cycle lifetime, with over 95% capacity retention, suggests that the system using solvated redox-active species shows excellent durability. The high coulombic efficiency of 95% indicates that self-discharge is mitigated on the timescale studied. In order to further study the self-discharge, we recorded the open circuit voltage (OCV) for 12 hours for a cell with [KI (0.3 M) + $VOSO_4$ (0.2 M)] electrolyte and a cell with H_2SO_4 electrolyte of a pH value of 2. The self-discharge of the electrolyte [KI (0.3 M) + $VOSO_4$ (0.2 M)] is, in fact, much less significant (Figure S5). Self-discharge of supercapacitors has been widely observed for redox-inert electrolytes. It is not surprising to see better results from a redox

electrolyte than an inert electrolyte, considering that a variety of mechanisms can lead to self-discharge.[37, 38] The results suggest that anionic catholyte and cationic anolyte in the electrolyte do not contribute extensively to self-discharge.

We next studied the mechanism for the enhanced charge storage. It is important to confirm whether the charging leads to the formation of new oxidized anions at the positive electrode and new reduced cations at the negative electrode. We polarized an H-cell (two half cells separated by a glass frit) filled with an electrolyte of [KI (0.3 M) + $VOSO_4$ (0.2 M)] at 1.0 V. At this cell voltage, the potential at the positive electrode goes up from the potential of zero charge (PZC) of the porous carbon electrode (0.42 V vs. standard hydrogen electrode (SHE)) to a voltage where I^- is likely oxidized to I_3^-. The potential at the negative electrode deviates from the PZC to a voltage where VO^{2+} could be reduced to V^{3+} (or to complex ions that contain V(III)). We expect that both catholyte and anolyte may contain I_3^- and V^{3+} since the ions diffuse within the H-cell. In UV-Vis spectra of the catholyte, new adsorption peaks of I_3^- at 286 nm and 352 nm are observed, compared to the original electrolyte (Figure. 3a). We have not observed the absorption of V^{3+} in the UV-Vis spectra. This may be due to strong adsorption of VO^{2+} and the overlapping absorption wavelengths for VO^{2+} and V^{3+}. UV-Vis spectra of related solutions are shown in Figures S6 – S10 and Table S2. Raman measurements show that the peak intensity of VO^{2+} decreases in anolyte, compared to the original electrolyte, suggesting that the VO^{2+} ions were consumed at negative electrode (Figure 3b and Figure S11).

We conducted mass spectroscopy (MS) analyses on catholyte, anolyte, and the original electrolyte. Interestingly, the primary anion and cation in the original electrolyte are identified as $[(VO^{2+})(I^-)_3]^-$ and $[(VO^{2+})_3\bullet(SO_4^{2-})_2\bullet H_2O]^{2+}$, respectively. The mass spectra of anions from catholyte and the original electrolyte are compared in Figures 4a and 4b. It is worth noting that a

peak at 381 was observed for the original electrolyte. We attribute it to@ I_3^- although we did not observe the I_3^- peak in the UV-Vis spectrum of the original electrolyte. This may be due to the very low concentration of the ion. New peaks at 399 and 624 are identified in the catholyte to be $[(I_3^-)(H_2O)]^-$ and $[(V^{3+})(HSO_4^-)\ (SO_4^{2-})(I_3^-)]^-$, respectively. The peak intensity at 381 was increased as well, corroborating the UV-Vis results. It is evident that I^- ions are oxidized into I_3^- that may or may not reside in the complex ions. The mass spectra of cations from anolyte and the original electrolyte are compared in Figures 4c and 4d. New peaks at 348, 539, 591 can be identified as $[(V^{3+})_2(O_2^0)(I^-)_4 \bullet 3H_2O]^{2+}$, $[(V^{3+})_2(O_2^0)_2(I_3^-)_2(SO_4^{2-}) \bullet 3H_2O]^{2+}$, and $[(V^{3+})(O_2^0)(I_3^-)(I^-)]^+$, respectively. Our results show that V(III) was formed during the polarization, and many newly-formed cations contain V(III) (detailed information is given in Tables S4 and S5). Digital photos of the H-cell before and after charging show that the catholyte color turned from blue to green (Figure S12). The chemical characterization data suggest that the majority of species in the catholyte are anionic and the majority in the anolyte are cationic, which is likely to be important for preventing self-discharge without an ion-selective membrane.

Conclusions

We have demonstrated a new strategy to use anolyte and catholyte in a simple EDLC configuration to store charge by both Faradaic and capacitive processes simultaneously. The mixed [KI+$VOSO_4$] electrolyte serves as the source for both anolyte and catholyte. Excellent cycling performance was demonstrated in the cell design. The energy storage mechanism of the new system using anolyte and catholyte was investigated by UV-Vis spectra and MS. Incorporating Faradaic energy storage using stable soluble redox species that are appropriately charged to be incorporated into the electric double layer likely enables the long cycling life and

improved energy densities. This approach represents a new route for device design that may be widely applicable for hybrid electrochemical battery-supercapacitor system.

Acknowledgments

This work was supported by Advanced Research Project Agency-E (ARPA-E), Department of Energy (DOE) of the United States (Award No. DE-AR0000344). This work made use of the Shared Experimental Facilities of the Materials Research Laboratory (MRL) at the University of California, Santa Barbara. The MRL Shared Experimental Facilities are supported by the MRSEC Program of the NSF under Award No. DMR 1121053; a member of the NSF-funded Materials Research Facilities Network (www.mrfn.org). We thank Prof. Michael T. Bowers for assistance with the MS analysis that is supported by NSF (CHE-0909743) and Waters Corp. for the donation of T-wave Q-TOF instrument; Dr. Christine Pastorek for UV-Vis measurements; Dr. May Nyman, Dr. Yu Hou, and Dr. Zuolei Liao for Raman analysis; and Dr. David Auston for his assistance in directing this research in close accordance with ARPA-e guidelines and the Materials Genome Initiative.

References

1. X. N. Xie, Y. Wang, Q. Wang, K. P. Loh, *Adv. Mater.*, **24**, 76 (2012).
2. B. Dunn, H. Kamath, J. M. Tarascon, *Science*, **334**, 928 (2011).
3. H. I. Becker, V. Ferry, *United States Patent*, 2800616 (1957).
4. M. Noked, A. Soffer, D. Aurbach, *J. Solid State Electrochem.*, **15**, 1563 (2011).
5. P. Simon, Y. Gogotsi, *Acc. Chem. Res.*, ***46***, 1094 (2013).
6. A. J. Smith, J. C. Burns, D. Xiong, J. R. Dahn, *J. Electrochem. Soc.*, **158**, A1136 (2011).
7. A. J. Bard, L. R. Faulkner, *Electrochemical Methods: Fundamentals and Applications*, *2nd Ed.* John Wiley and Sons (2001).
8. P. Simon, Y. Gogotsi, *Nat. Mater.*, **7**, 845 (2008).
9. L. Hu, M. Pasta, F. L. Mantia, L. Cui, S. Jeong, H. D. Deshazer, J. W. Choi, S. M. Han, Y. Cui, *Nano Lett.*, **10**, 708 (2010).
10. M. Kaempgen, C. K. Chan, J. Ma, Y. Cui, G. Gruner, *Nano Lett.*, **9**, 1872 (2009).
11. J. Chmiola, G. Yushin, Y. Gogotsi, C. Portet, P. Simon, P. L. Taberna, *Science*, **313**, 1760 (2006).
12. C. Merlet, B. Rotenberg, P. A. Madden, P. L. Taberna, P. Simon, Y. Gogotsi, M. Salanne, *Nat. Mater.*, **11**, 306 (2012).
13. M. D. Stoller, S. Park, Y. Zhu, J. An, R. S. Ruoff, *Nano Lett.*, **8**, 3498 (2008).
14. Y. Zhu, S. Murali, M. D. Stoller, K. J. Ganesh, W. Cai, P. J. Ferreira, A. Pirkle, R. M. Wallace, K. A. Cychosz, M. Thommes, D. Su, E. A. Stach, R. S. Ruoff, *Science*, **332**, 1537 (2011).
15. M. F. El-Kady, V. Strong, S. Dubin, R. B. Kaner, *Science*, **335**, 1326 (2012).

16. M. F. El-Kady, R. B. Kaner, *Nat. Commun.*, **4**, 1475 (2013).

17. J. A. Lee, M. K. Shin, S. H. Kim, H. U. Cho, G. M. Spinks, G. G. Wallace, M. D. Lima, X. Lepro, M. E. Kozlov, R. H. Baughman, S. J. Kim, *Nat. Commun.*, **4**, 1970 (2013).

18. W. T. Gu, M. MaSevilla, A. Magasinski, A. B. Fuertes, G. Yushin, *Energy Environ. Sci.*, **6**, 2465 (2013).

19. W. J. Yuan, Y. Zhou, Y. R. Li, C. Li, H. L. Peng, J. Zhang, Z. F. Liu, L. M. Dai, G. Q. Shi, *Sci. Rep.*, **3**, 2248 (2013).

20. B. E. Conway, *J. Electrochem. Soc.*, **138**, 1539 (1991).

21. H. Y. Lee, J. B. Goodenough, *J. Solid State Chem.*, **144**, 220 (1999).

22. T. Brezesinski, J. Wang, S. H. Tolbert, B. Dunn, *Nat. Mater.*, **9**, 146 (2010).

23. K. Brezesinski, J. Wang, J. Haetge, C. Reitz, S. O. Steinmueller, S. H. Tolbert, B. M. Smarsly, B. Dunn, T. Brezesinsk, *J. Am. Chem. Soc.* **132**, 6982 (2010).

24. T. Brezesinski, J. Wang, R. Senter, K. Brezesinski, B. Dunn, S. H. Tolbert, *ACS Nano*, **2**, 967 (2010).

25. S. W. Lee, N. Yabuuchi, B. M. Gallant, S. Chen, B. S. Kim, P. T. Hammond, Y. Shao-Horn, *Nature Nanotech.*, **5**, 531 (2010).

26. G. G. Amatucci, F. Badway, A. D. Pasquier, T. Zheng, *J. Electrochem. Soc.*, **148**, A930 (2001).

27. B. Wang, J. S. Chen, Z. Y. Wang, M. Srinivasan, X. W. Lou, *Adv. Energy Mater.*, **2**, 1188 (2012).

28. G. Q. Zhang, B. Y. Xia, C. Xiao, L. Yu, X. Wang, Y. Xie, X. W. Lou, *Angew. Chem. Int. Ed.*, **52**, 8643 (2013).

29. G. Lota, E. Frackowiak, *Electrochem. Commun.*, **11**, 87 (2009).

30. S. Roldán, C. Blanco, M. Granda, R. Menéndez, R. Santamaría, *Angew. Chem. Int. Ed.,* **50**, 1699 (2011).

31. E. Frackowiak, K. Fic, M. Meller, G. Lota, *ChemSusChem*, **5**, 1181 (2012).

32. J. A. Maciá-Agulló, B. C. Moore, D. Cazorla-Amorós, A. Linares-Solano, *Carbon*, **42**, 1367 (2004).

33. S. Roldán, M. Granda, R. Menéndez, R. Santamaría, C. Blanco, *J. Phys. Chem. C*, **115**, 17606 (2011).

34. Y. Li, Z. Huang, K. Huang, D. Carnahan and Y. Xing, *Energy Environ. Sci.*, **6**, 3339 (2013).

35. K. Huang, Y. Li, Y. Xing, *Electrochimica Acta*, **103**, 44 (2013).

36. G. Yu, L. Hu, M. Vosgueritchian, H. Wang, X. Xie, J. R. McDonough, X. Cui, Y. Cui, Z. Bao, *Nano Lett.*, **11**, 2905 (2011).

37. X. Zhang, X. Wang, L. Jiang, H. Wu, C. Wu, J. Su, *J. Power Sources*, **216**, 290 (2012).

38. Y. Lin, N. Wu, *J. Power Sources*, **196**, 851 (2011).

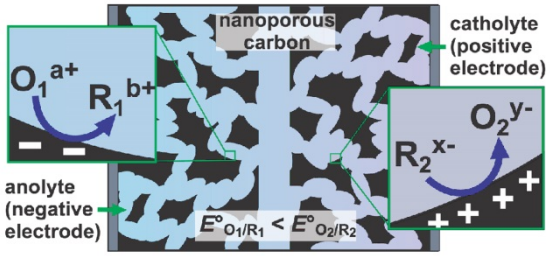

Figure 1. Schematic illustration of the proposed capacitive and Faradaic energy-storage processes occurring on the two electrodes.

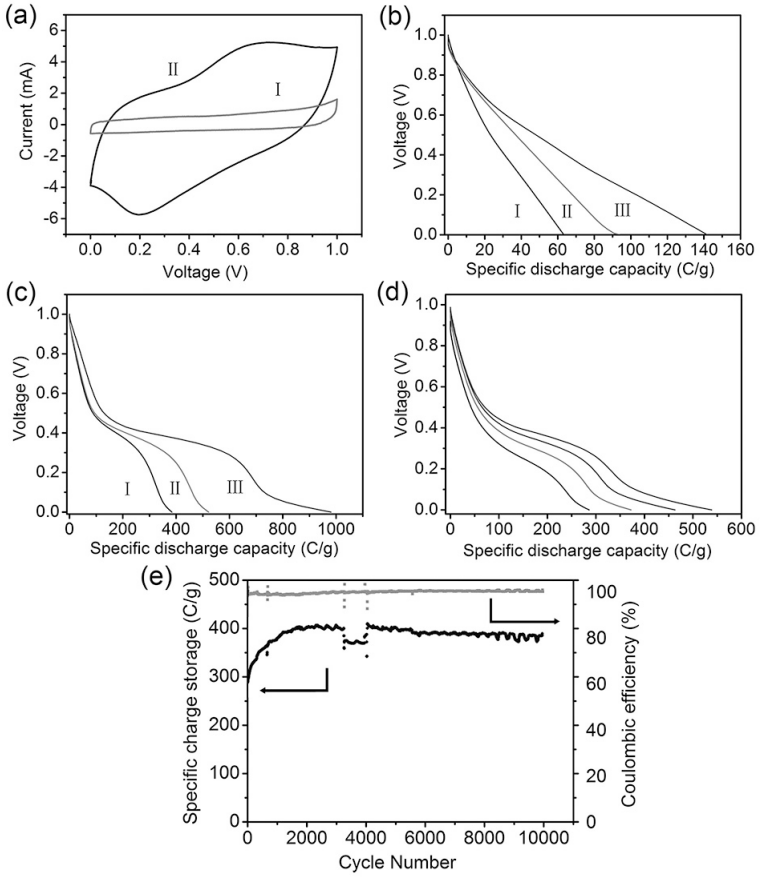

Figure 2. (a) Cyclic voltammetry (20 mV/s) of cells with different electrolytes, I) H_2SO_4 (1 M), II) [KI (0.15 M) + $VOSO_4$ (0.1 M)]; **(b)** Galvanostatic discharge profiles of cells with different electrolytes I) H_2SO_4 (1 M), II) KI (0.15 M), III) $VOSO_4$ (0.1 M) at the current rate of 1 A/g; **(c)** Galvanostatic discharge profiles of the I) [KI (0.15 M) + $VOSO_4$ (0.1 M)], II) [KI (0.3 M) + $VOSO_4$ (0.2 M)], III) [KI (0.75 M) + $VOSO_4$ (0.5 M)] cells at the current rate of 1 A/g; **(d)** Discharge profiles of the [KI (0.3 M) + $VOSO_4$ (0.2 M)] cell at different discharge rates, from right to left: 1, 2, 4, and 8 A/g, respectively; **(e)** Galvanostatic cycling profiles of the [KI (0.3 M) + $VOSO_4$ (0.2 M)] cell at 4 A/g.

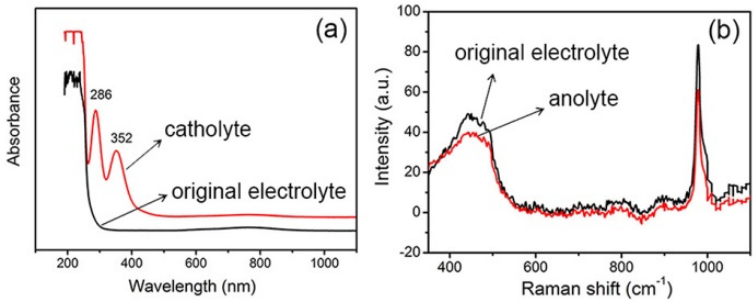

Figure 3. **(a)** UV-Vis spectra of the original electrolyte and catholyte (diluted 10:1 with water); **(b)** Raman spectra of the original electrolyte and anolyte.

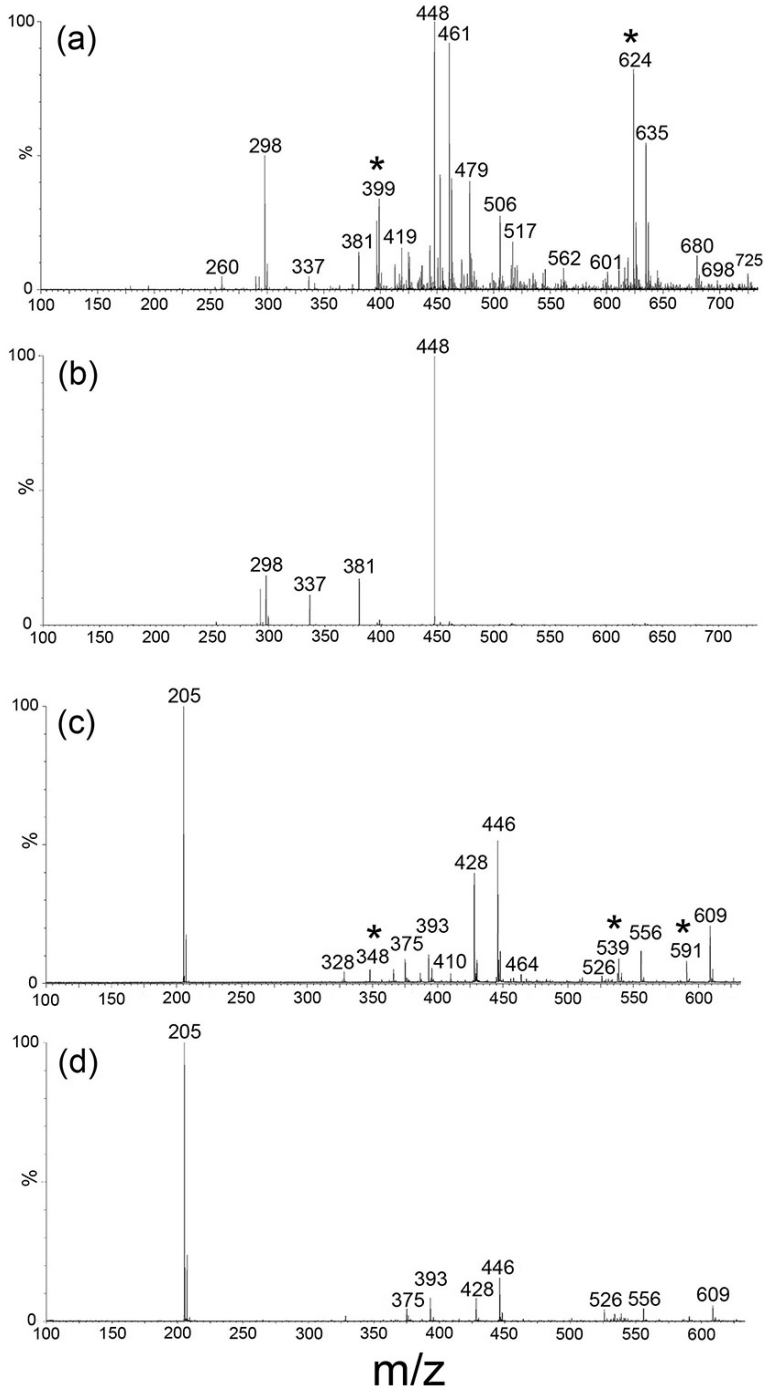

Figure 4. Mass spectra of anions in catholyte **(a)** and the original electrolyte **(b)**; and cations in anolyte **(c)** and the original electrolyte **(d)**. Charging was carried out by polarizing the cell at 1 V for 1 hour before the measurements.

Figure Captions

Figure 1. Schematic illustration of the proposed capacitive and Faradaic energy-storage processes occurring on the two electrodes.

Figure 2. (a) Cyclic voltammetry (20 mV/s) of cells with different electrolytes, I) H_2SO_4 (1 M), II) [KI (0.15 M) + $VOSO_4$ (0.1 M)]; (b) Galvanostatic discharge profiles of cells with different electrolytes I) H_2SO_4 (1 M), II) KI (0.15 M), III) $VOSO_4$ (0.1 M) at the current rate of 1 A/g; (c) Galvanostatic discharge profiles of the I) [KI (0.15 M) + $VOSO_4$ (0.1 M)], II) [KI (0.3 M) + $VOSO_4$ (0.2 M)], III) [KI (0.75 M) + $VOSO_4$ (0.5 M)] cells at the current rate of 1 A/g; (d) Discharge profiles of the [KI (0.3 M) + $VOSO_4$ (0.2 M)] cell at different discharge rates, from right to left: 1, 2, 4, and 8 A/g, respectively; (e) Galvanostatic cycling profiles of the [KI (0.3 M) + $VOSO_4$ (0.2 M)] cell at 4 A/g.

Figure 3. (a) UV-Vis spectra of the original electrolyte and catholyte (diluted 10:1 with water); (b) Raman spectra of the original electrolyte and anolyte.

Figure 4. Mass spectra of anions in catholyte (a) and the original electrolyte (b); and cations in anolyte (c) and the original electrolyte (d). Charging was carried out by polarizing the cell at 1 V for 1 hour before the measurements.